JOURNAL OF MATERIALS SCIENCE 18 (1983) 2274–2282

Fracture toughness of composite adherend adhesive joints under mixed mode I and III loading

E. J. RIPLING, J. S. SANTNER, P. B. CROSLEY
Materials Research Laboratory, 1 Science Road, Glenwood, Illinois 60425, USA

A tapered double cantilever beam specimen was modified in order to evaluate the fracture toughness of scarf joints. The modification was relatively simple: the bond line which is normally perpendicular to the applied load with this type of specimen was inclined to form the scarf joint. With this change, both normal and shear components of force act on the crack plane. Hence, in addition to measuring the total strain energy release rate, $\mathcal{G}_{total}$, its two components, the opening mode toughness, $\mathcal{G}_{I}$, and the edge shearing or tearing toughness, $\mathcal{G}_{III}$, were measured as well. In spite of the fact that the separation loads increased continuously with increasing scarf angle, or over-lap length, $\mathcal{G}_{total}$ and $\mathcal{G}_{III}$ only increased so long as the ratio of over-lap length to thickness did not exceed 1.75:1. Further increases in over-lap length decrease the toughness because of separation of fibres within the composite adherends.

1. Introduction

Adhesive bonds fracture by progressive separations that initiate at pre-existing cracks or crack-like defects. These defects may be introduced into the bond line during joint fabrication, or they may develop in service because of exposure to an aggressive environment, and/or to fatigue loading.

A large body of information has been developed over the past decade or two on the fracturing of adhesive bonds. These studies have been mainly concerned with opening mode cracking, although a few tests have also been made on mixed mode I and II cracking [1], and an even smaller number of tests have been made on mixed mode I and III cracking [2].

An understanding of mixed mode cracking, and especially cracking under modes I and III, is important for developing fracture control plans for composite structures. When composite are adhesively bonded, step joints are generally used in which the steps are fine enough so that its shape approaches that of a scarf joint. These joints are generally much longer in the direction perpendicular to the applied load than they are parallel to the applied load so that crack extension occurs under a mixed opening and edge-shearing mode, i.e. modes I and III, as shown in Fig. 1. Hence, test specimens for evaluating adhesives for composite–composite or composite–metal joints must develop combinations of these modes. None of the fracture specimens developed for evaluating adhesive joints are especially well suited for this purpose. Hence, this programme was undertaken to develop a specimen for studying the behaviour of flawed joints subjected to modes I to III loading. This programme must be considered a preliminary study and recommendations for further study are contained in the last section.

2. Test materials

A single 305 mm × 305 mm (12 in × 12 in) plate of graphite–epoxy composite, 2.8 mm (0.109 in) thick, was used for this programme. The plate had a lay-up pattern of $[+45/-45/0/90/0/-45/+45]_3$. Some compliance measurements were also made using 2024-T351 adherends which were 3.1 mm (0.121 in) thick.

The adhesive was a scrim-supported generically modified epoxy, AF-163-2K (2.034 g m^{-2} or 0.06 oz ft^{-2}) manufactured by the 3M Company.

0022–2461/83 $03.00 + .12

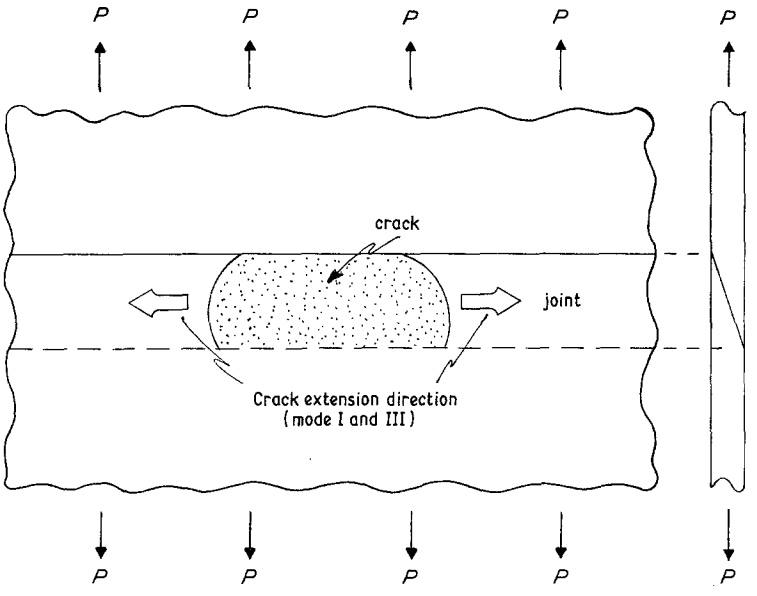

Figure 1 Schematic diagram of mode I and mode III crack growth in a scarf joint.

3. Test specimen

Structural adhesives crack under a high level of triaxiality, because the high modulus adherends prevent the adhesive from contracting. In spite of this, they do not exhibit a "pop" of the type frequently found in high strength metals that fracture in plane strain so that their toughness cannot be described by an abrupt instability of the type generally associated with plane strain fracture toughness testing. Earlier studies of adhesive fracturing have used the strain energy release rate, $\mathcal{G}$, associated with stable cracking as the measure of fracture toughness, and defined this as $\mathcal{G}_{Ic}$ [3]. This can be measured most easily with a linear compliance specimen such as the tapered double cantilever beam (TDCB) specimen. Stable cracking is exhibited with this type of specimen when the cracking load remains constant as a function of displacement or time. This occurs because $\mathcal{G}$ is independent of crack length, and a function of applied load only. This unique feature facilitates the measurement of critical values of $\mathcal{G}$, so this specimen type was modified to allow for mixed mode I and III cracking for the present study.

The TDCB specimen shape is defined by a single number, identified as m, having the dimensions of 1/length [4]. The value of m defines the dependence of specimen height (h) on crack length (a) for uniformly thick adherends. The higher the m number, the smaller the test specimen height at a given crack length. For this programme, m was chosen as $1.18\,mm^{-1}$ ($30\,in^{-1}$), which resulted in a specimen that was as small as was thought reasonable for composite adherends.

In order to simulate the combined mode I and III cracking found in composite–composite or composite–metal joints, the edges to be joined were tapered to form a scarf joint, as shown in Fig. 2. The ratio of mode III to mode I cracking increases as the scarf angle, θ, increases. The shape of a specimen as described by m is restricted to adherends having a rectangular cross-section because the expression used for the moment of inertia, I, in calculating compliance, assumes such an adherend shape. For other cross-sections such as the one used here, the shape factor must be based on a value of I that takes into account both the portion of the adherend that does not change with a, i.e. the triangular portion, as well as the rectangular portion that does change with a. The shape factor for these more complex cross-sections has been designated m_0 in [5]. In spite of the fact that the specimen shape should have been based on an m_0 type of calculation, modifying the specimen contour for each scarf angle would have increased specimen machining costs as well as the complexity of the jig used for specimen bonding. Hence, all specimens were machined to the same contour. This produced only a negligible error in calculating $\mathcal{G}$ when θ was small; however, the error became large enough to require a correction when the scarf angle was large, as is discussed below.

To evaluate the specimen compliance, it was necessary to accurately measure displacements

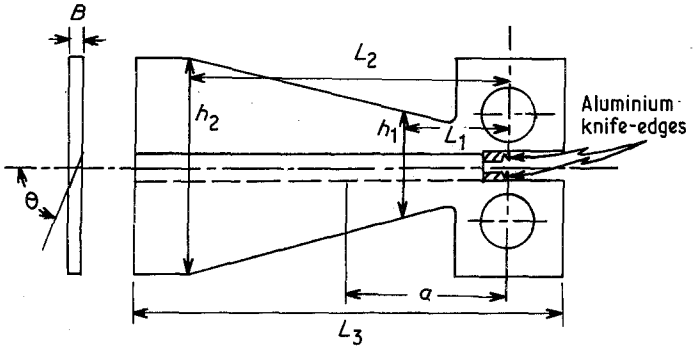

Figure 2 Dimensions of test specimen ($m = 1.18\,mm^{-1}$; $30\,in^{-1}$).

mm	inch		mm	inch
L_1 = 25.4	1.0	h_1	25.4	1.0
L_2 = 76.2	3.0	h_2	50.8	2.0
L_3 = 101.6	4.0			
B = 2.8	0.109 for composite			
B = 3.1	0.121 for aluminium			

at the load-line while the specimen was being loaded. A standard clip-gauge of the type used for toughness testing according to ASTM Test Method E399 [6] was used, and this requires a knife-edge to hold it in place. It was not practical to machine the knife-edge into the composite so that small aluminium knife-edges, as shown by the cross-hatched section in Fig. 2, were bonded to the cut-out section for this purpose.

The first few specimens that were fabricated were unsatisfactory, because the bond line was too thin and had a number of voids. After a number of trials, it was found that a satisfactory bond thickness could be produced by using two layers of adhesive with a bond pressure of about 0.14 MPa (20 psi) and a 1 h cure at 149° C (300° F). The number of voids were reduced to a reasonable number of pre-conditioning the adherends at 149° C (300° F) for 1 h.

In order to minimize machining costs, the adherends were also re-used. After each specimen was tested, the adhesive was machined off the bond surface. For small scarf angles, the specimen could be used a half dozen times or more. For larger angles, where the loads were high, the adherends showed some evidence of damage after three or four uses.

4. Compliance calibration

As stated above, the test specimen was designed to an m value of $1.18\,mm^{-1}$ ($30\,in^{-1}$). Experience has shown that while specimens fabricated to a contour defined by m (or m_0) exhibit a linear dependence of compliance on crack length, the predicted dC/da may not be the same as the measured value [7]. An additional concern with composite adherends is that their bending modulus is sensitive to the ratio of span length to beam height [8]. Hence, the specimen was compliance calibrated to determine m', the experimentally derived value of m. Two groups of specimens were prepared, one using composite adherends, and the other using an aluminium alloy. Most of the compliance calibration was done on specimens having a scarf angle, θ, of zero degrees. The calibration procedure consisted of preparing the specimen in the normal manner with a piece of teflon tape on the bond line. The length of the teflon tape was varied to simulate various crack lengths. Each specimen was loaded and unloaded to get four load, P, against displacement, Δ, curves. The specimen was then turned upside down and four more curves were collected. These eight values of compliance were averaged to get one value of compliance, C, at each crack length, a.

Seven different crack lengths were used for the composite adherends with a scarf angle of 0°. Only two different crack lengths were used for scarf angles of 45°, 60° and 75°. All the compliance data collected with composite adherends, along with the expressions for C against a, are shown in Fig. 3. Of course, only the 0° data have enough points to define dC/da with any reasonable degree of accuracy. Even these limited data show that the values of dC/da are not much different for 0°, 45° and 60° scarf joints, but the absolute values of C for the 60° and 75° joints are markedly lower than that of the 0° and 45° joints.

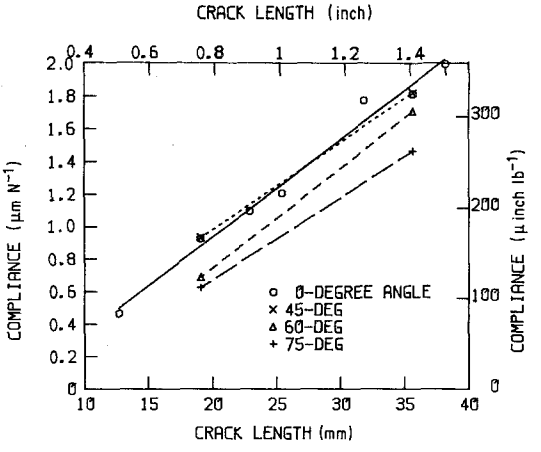

Scarf angle	Expression
0°	$C = (-0.2631 + 0.0601\,a)\ \mu m\ N^{-1}$
45°	$C = (-0.08478 + 0.0536\,a)\ \mu m\ N^{-1}$
60°	$C = (-0.4819 + 0.0616\,a)\ \mu m\ N^{-1}$
75°	$C = (-0.3404 + 0.0508\,a)\ \mu m\ N^{-1}$

Figure 3 Compliance of composite adherend specimen as a function of crack length.

Similar data were collected using aluminium adherends. These data and the dependence of C on a is shown in Fig. 4. For specimens made with the two higher scarf angles, 60° and 75°, the adherends deformed plastically so that these data were not used.

Using a value of Young's modulus of 73 GPa (10.6×10^6 psi), and the thickness of the aluminium alloy, 3.1 mm (0.121 in), m' was found to be $1.48\ mm^{-1}$ ($38\ in^{-1}$). This value is obviously a great deal higher than the calculated one of $1.18\ mm^{-1}$ ($30\ in^{-1}$).

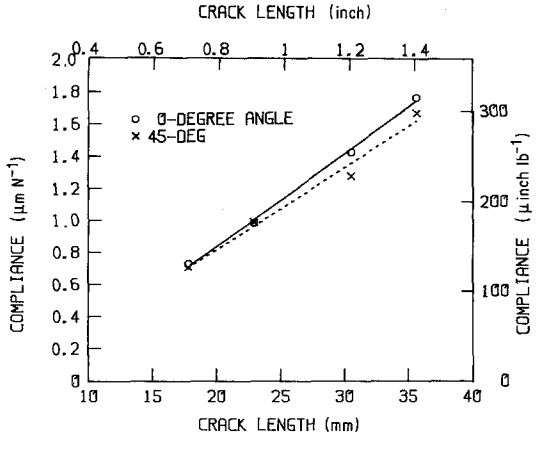

Scarf angle	Expression
0°	$C = (-0.3209 + 0.0581\,a)\ \mu m\ N^{-1}$
45°	$C = (-0.2087 + 0.0514\,a)\ \mu m\ N^{-1}$

Figure 4 Compliance of aluminium adherend specimens as a function of crack length.

The bending modulus of the composite was not measured. It was calculated, however, using the composite measured thickness of 2.8 mm (0.109 in) and the value of $m' = 1.48\ mm^{-1}$ ($38\ in^{-1}$). This gave a modulus of 76.7 GPa (11.1×10^6 psi), or almost the same as that of the aluminium alloy.

Since not enough data were collected on the larger scarf angles to obtain a useful value of dC/da, some calculations were carried out to determine the error in using the dC/da value obtained for 0°. This was done by modelling the DCB specimen as a pair of cantilever beams which deform only by bending. In this case, the compliance change is given by

$$\frac{dC}{da} = \frac{2a^2}{EI} \tag{1}$$

where E is Young's modulus and I is the moment of inertia of one of the beam arms at the crack tip location. Advantage is taken of this relationship in designing linear compliance change specimens; the specimens are shaped so that I increases in direct proportion to a^2.

The beam cross-section in a scarf joint specimen is trapezoidal rather than rectangular, as shown in Fig. 5. When the scarf angle is zero, the moment of inertia through the centroid of a rectangular cross-section is

$$I_R = BH/12 \tag{2}$$

This expression becomes increasingly incorrect as the scarf angle is increased and is most severe at short crack lengths when H is smallest. The proper expression for the trapezoid is

$$I_T = \frac{BH^3}{12}(1 + 2\beta^2 - \tfrac{1}{3}\beta^4) \tag{3}$$

where $\beta = 0.5\,(B/H)\tan\theta$. The term in brackets is clearly a correction factor to the moment of inertia for the rectangular cross-section. Since dC/da is inversely proportional to I the correction factor for dC/da is

$$k = I_R/I_T = (1 + 2\beta^2 - \tfrac{1}{3}\beta^4)^{-1} \tag{4}$$

The correction factor, k, is plotted in Fig. 6 as a function of a for values of θ which were used in this programme.

The most accurate calculation of joint tough-

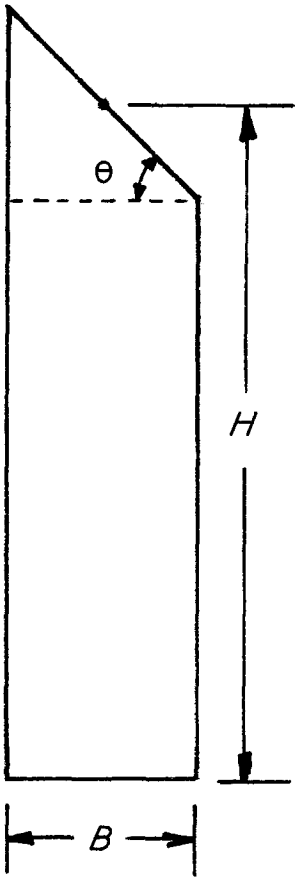

Figure 5 Adherend dimensions.

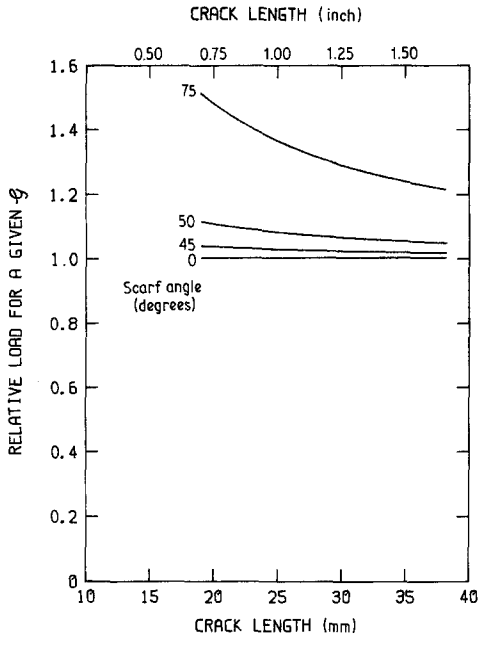

Figure 6 Calculated correction factors on compliance (and $\mathcal{G}$) as a function of crack length and scarf angle.

ness would be made by calculating $\mathcal{G}$, assuming rectangular cross-sectioned adherends, and correcting these values by using the appropriate value of k for each crack length. For the three smallest scarf angles, 0°, 45° and 60°, the correction is less than 10% for all crack lengths of interest, and hence no correction was made in the course of data reduction. For the 75° scarf angle joints, the calculated value of $\mathcal{G}$ based on rectangular cross-sectioned adherends was reduced by 25% for all crack lengths. This again gave an error of less than 10% over the range of crack lengths that were used.

5. Test results

5.1. Method of analysis

The scarf joints made it possible to calculate three values of $\mathcal{G}$ (critical), $\mathcal{G}$ (total) and its two components: $\mathcal{G}$ for a tearing mode, and $\mathcal{G}$ for an opening mode. These are identified as $\mathcal{G}_{Tc}$, $\mathcal{G}_{III}$ and $\mathcal{G}_{I}$, respectively*. The expressions for calculating these quantities are shown in Fig. 7.

5.2. Load P against displacement Δ curves

The shape of typical P–Δ curves for each of the scarf angles is shown in Figs. 8 to 11. It is apparent that all specimens exhibited a load plateau, i.e. showed stable cracking. (The initial load peak is ignored, since it is caused by the blunt starter crack produced by the teflon tape. As the crack extends, its tip takes on the shape associated with a running crack.)

For the 0°, 45° and 60° scarf angle specimens, the variation in critical load, P_c, was about ± 5%, which gave a variation of ± 10% in $\mathcal{G}_{Tc}$. This amount of scatter is not uncommon for adhesives. For the 75° joints, the load variation beyond the peak was somewhat higher, but this added scatter was associated with a tendency of the load to decrease with crack length. This negative sloping P–Δ curve is necessary to maintain a constant value of $\mathcal{G}$ because of the pronounced negative slope of the 75% scarf angle specimen curve in Fig. 6.

5.3. Fracture toughness

Equation 1 in Fig. 7 was used to calculate $\mathcal{G}_{Tc}$. The value P_{Tc} was taken as the average plateau

*The symbols $\mathcal{G}_{Ic}$ and $\mathcal{G}_{IIIc}$ were reserved for fracturing under pure mode I or III loading.

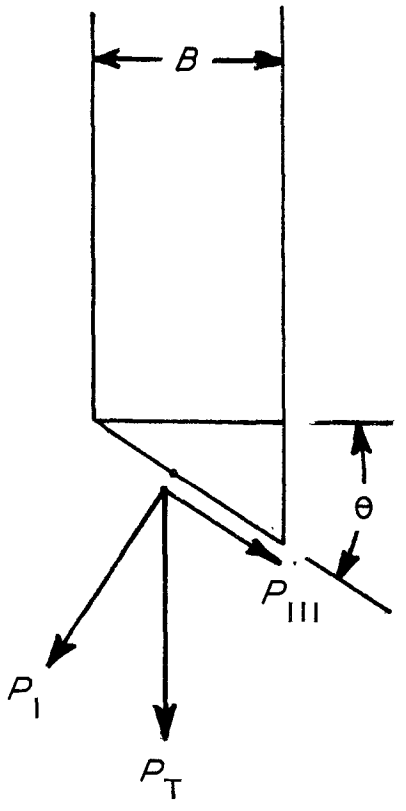

$$\mathcal{G} = \frac{P^2}{2B}\frac{dC}{da}$$

$$B_S = \frac{B}{\cos\theta}$$

$$\mathcal{G}_T = \frac{P_T^2}{2B_S}\frac{dC}{da} = \frac{\cos\theta}{2}\frac{P_T^2}{B}\frac{dC}{da} \quad (5)$$

$$P_I^2 = (P_T\cos\theta)^2 \qquad P_{III}^2 = (P_T\sin\theta)^2$$

$$\mathcal{G}_I = \frac{\cos^3\theta}{2}\frac{P_T^2}{B}\frac{dC}{da} = \mathcal{G}_T\cos^2\theta \quad (6)$$

$$\mathcal{G}_{III} = \frac{\cos\theta\sin^2\theta}{2}\frac{P_T^2}{B}\frac{dC}{da} = \mathcal{G}_T\sin^2\theta \quad (7)$$

Figure 7 Calculation of $\mathcal{G}_T$, $\mathcal{G}_I$ and $\mathcal{G}_{III}$.

load for all the specimens having the same scarf angle; dC/da was taken as $0.06\,\mu m N^{-1}$ ($270\,\mu in\,lb^{-1}$) for the 0°, 45° and 60° joints (see Fig. 3), and $0.045\,\mu m N^{-1}$ ($200\,\mu in\,lb^{-1}$) for the 75° joints (see Fig. 6). The two components were obtained by multiplying $\mathcal{G}_{Tc}$ by either $\cos^2\theta$ or $\sin^2\theta$ as appropriate.

The three toughness parameter, normalized to $\mathcal{G}_{Ic}$, are shown as a function of scarf angle in Fig. 12. $\mathcal{G}_{Tc}/\mathcal{G}_{Ic}$ increased by 60% as the scarf angle was increased from 0° to 60°, but a further

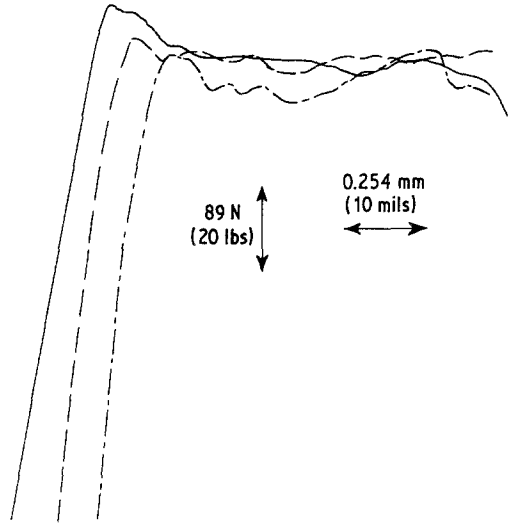

Figure 8 Load, P, against displacement, Δ, for 0° scarf angle specimens.

increase of scarf angle to 75° produced a drop in toughness. $\mathcal{G}_{III}/\mathcal{G}_{Ic}$ follows the same shape as the $\mathcal{G}_{Tc}/\mathcal{G}_{Ic}$ curve since $\mathcal{G}_{III}$ is the dominant component of $\mathcal{G}_{Tc}$ beyond 45° scarf angle. $\mathcal{G}_I/\mathcal{G}_{Ic}$ decreased continuously with scarf angle.

An increase in $\mathcal{G}_T$ and $\mathcal{G}_{III}$ with scarf angle might be expected, since fracture resistance is generally greater for shear mode loading than for opening mode. The decrease in $\mathcal{G}_T$ and $\mathcal{G}_{III}$ on going from the 60° to the 75° scarf angle, which might not be anticipated, may be the consequence

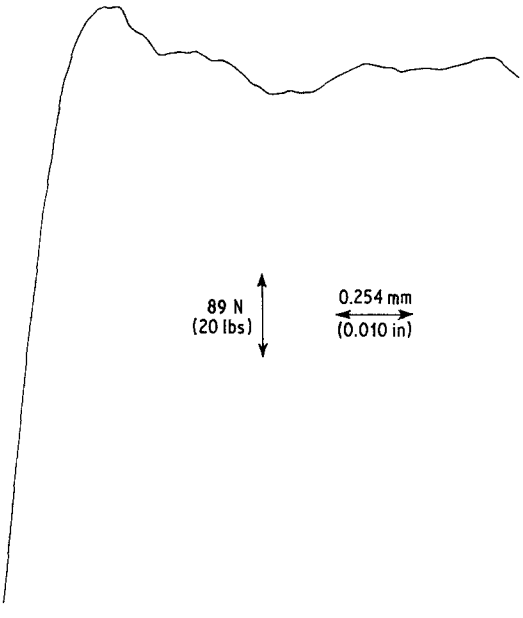

Figure 9 Load, P, against displacement, Δ, for 45° scarf angle specimens.

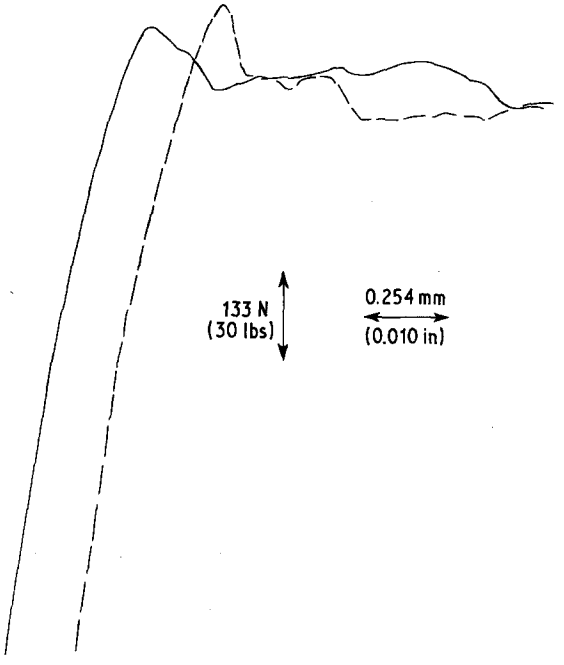

Figure 10 Load, P, against displacement, Δ, for 60° scarf angle specimens.

of a rapid change in geometrical configuration which allows for more exposure of the fibre–matrix interface, and hence more separation at this location. The fracture appearance, described below, is consistent with this view.

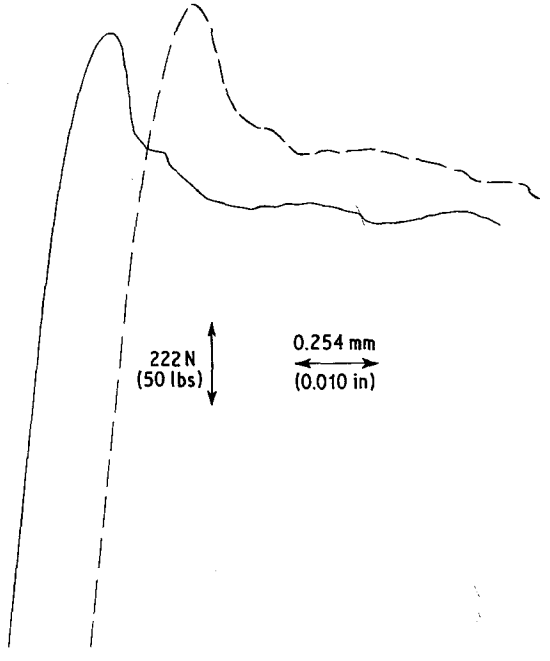

Figure 11 Load, P, against displacement, Δ, for 75° scarf angle specimens.

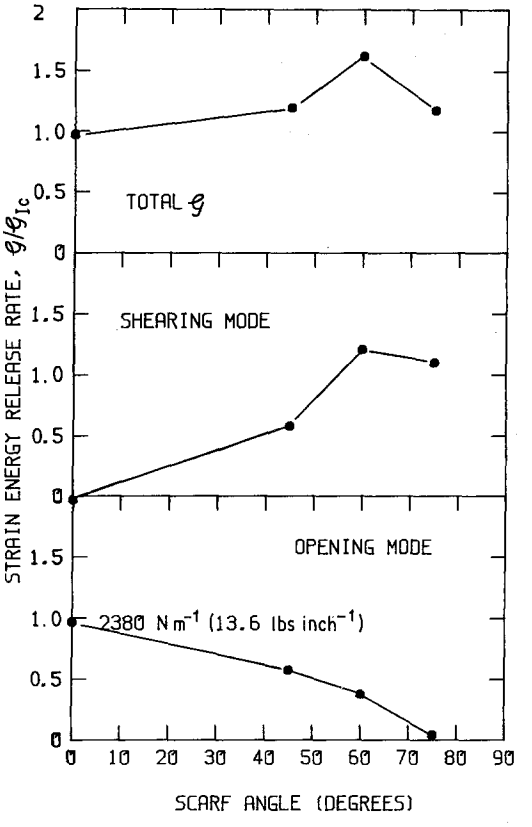

Figure 12 Fracture toughness of composite adherend bonds as a function of scarf angle.

The dependence of $\mathcal{G}_I$ on $\mathcal{G}_{III}$ is shown in Fig. 13. The addition of some tearing mode obviously decreased the value of $\mathcal{G}_I$ needed for fracture. The rate at which $\mathcal{G}_I$ drops is not so fast as to imply that $\mathcal{G}_{Tc}$ is a constant, however; on the other hand, the addition of $\mathcal{G}_{III}$ is more damaging than the reported effect of adding $\mathcal{G}_{II}$ to $\mathcal{G}_I$ for similar adhesives [2].

6. Fracture morphology

The fracture surface appearance changed in a reasonably systematic manner with scarf angle.

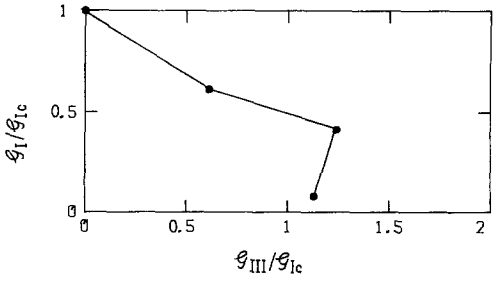

Figure 13 Dependence of $\mathcal{G}_I$ on $\mathcal{G}_{III}$.

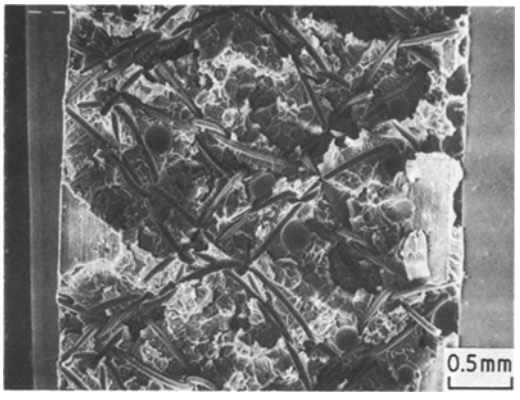

Figure 14 Typical fracture appearance of 0° scarf angle specimen (30 ×).

Starting with the 0° scarf angle specimens, separation occurred near the centre of the bond, Fig. 14, much like the separation reported earlier for metal adherend specimens [9]. As the scarf angle increased, the fracture tended to occur closer to one of the adhesive–adherend interfaces, although there was still evidence on both fracture surfaces for the 60° scarf angle specimen, as shown in Fig. 15. Along with this shifting of the fracture location, some of the fibres began pulling out as the scarf angle increased. For the 45° specimens, only a few fibres, parallel with the bond line, (i.e. 0° orientation) were pulled out, while at 60°, pull-out of the 0° degrees fibres near the fracture surface was almost complete, Fig. 15. Increasing the angle from 60° to 70° continued this process. At this

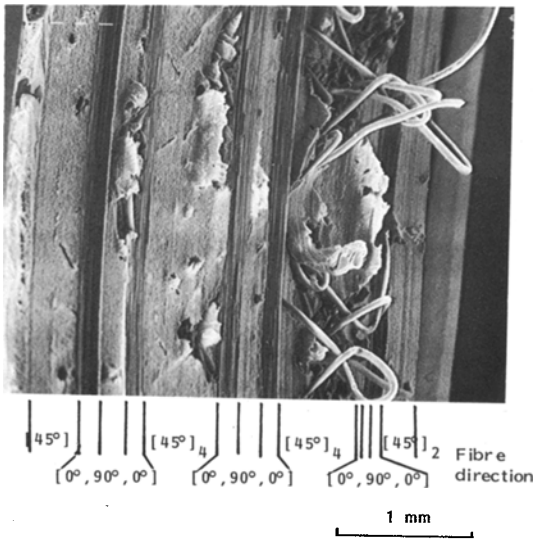

Figure 15 Typical fracture appearance of 60° scarf angle specimen (30 ×).

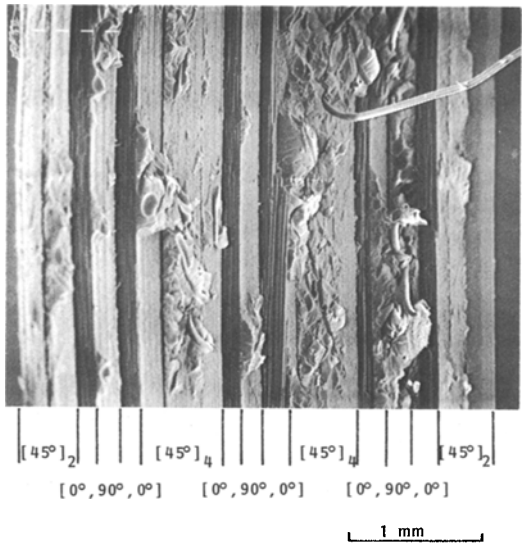

Figure 16 Typical fracture appearance of 75° scarf angle specimen (30 ×).

angle most of the fractures appeared to be at the interface, with almost no evidence of adhesive on one adhered, and the amount of fibre pull-out was still more severe, Fig. 16. It is this change from a cohesive to an adhesive fracture that probably accounts for the saturation of $\mathcal{G}_{Tc}$ at the 60° scarf angle in Fig. 12.

7. Conclusions and recommendations

1. A modified TDCB specimen was shown to be satisfactory for evaluating mixed mode I and III crack extension of the type that occurs in step joints of composite–adhesive–composite or composite–adhesive–metal systems. The modification consisted of changing the cross-section of the adhered from a rectangular to a trapezoid so that the bond became a scarf joint rather than a butt joint.

2. As the scarf angle, θ, increased, i.e. as the angle was changed to increase the overlap length of the joint, $\mathcal{G}$ increased. The increase was about 60% as the scarf angle increased from 0° to 60°. A further increase to 75° resulted in a decrease of $\mathcal{G}_{Tc}$ (although the fracture load, P_c, continued to increase. When $\mathcal{G}_{Tc}$ was resolved into opening mode I, and tearing, mode III, the former decreased, while the latter increased with scarf angle. The addition of $\mathcal{G}_{III}$ reduced the critical value of $\mathcal{G}_I$ at a rate much faster than had been previously shown for the influence of $\mathcal{G}_{II}$ on $\mathcal{G}_I$.

3. The fracture morphology changed with scarf angle, (i.e. with ratio of $\mathcal{G}_I/\mathcal{G}_{III}$). For pure mode

I, cracking was centre-of-bond; as θ increased, the crack tended toward the adherend–adhesive interface, and the amount of fibre pull-out increased. As the scarf angle increased from 60° to 75°, the fracture changed from cohesive (within the adhesive) to adhesive. This is probably the reason why $\mathcal{G}_{Tc}$ decreased over this range of scarf angle.

4. The specimen shape was not adjusted to account for the scarfed portion of the adherend. Additional testes should be conducted with specimens having this adjustment.

5. Additional tests should also be run with adherends that do not contain fibres that are parallel with the bond surface to determine how much tougher joints might be if fibre pull-out were minimized.

References

1. L. B. GRESZCSUK and A. B. MACANDER, in "Joining of Composite Materials", ASTM STP 749, edited by K. T. Keward (American Society for Testing and Materials, Philadelphia 1981) pp. 75–96.
2. SHELDON MOSTOVOY, S. T. CHIU and T. R. BRUSSAT, "Fracture Mechanics for Structural Adhesive Bonds – Final Reports", AFML TR 77-163, (Air Force Materials Laboratory, Wright-Patterson Air Force Base, Ohio, 1977).
3. E. J. RIPLING, S. MOSTOVOY and H. T. CORTEN, *J. Adhes.* **3** (1971) 107.
4. S. MOSTOVOY, P. B. CROSLEY and E. J. RIPLING, *ASTM J. Mater.* **2** (3) (1967) 661.
5. E. J. RIPLING, Final Report on Sub-Contract on ESR Steel Characterization, Battelle Columbus Laboratories Contract R-4255 (6622-4402), February 1980).
6. Standard Test Method for Plane-Strain Fracture Toughness of Metallic Materials, ANSI/ASTM E399-78a, American National Standards Institute and American Society for Testing and Materials.
7. P. B. CROSLEY and E. J. RIPLING, *ASTM STP* 627 (1977) 372.
8. E. J. RIPLING and J. S. SANTNER, "Fracture of Metal–Adhesive–Composite and Composite–Adhesive–Composite Systems", National Aeronautics and Space Administration (Lewis Research Center), October 1980.
9. S. MOSTOVOY and E. J. RIPLING, *J. Appl. Polymer Sci.* **10** (1966) 1351.

Received 21 September
and accepted 29 November 1982